Subunit Structure of Paired Helical Filaments in Alzheimer's Disease

C. M. WISCHIK,*‡ R. A. CROWTHER,* MURRAY STEWART,* and MARTIN ROTH‡
*Medical Research Council Laboratory of Molecular Biology, Hills Road, Cambridge CB2 2QH, England, and ‡Department of Psychiatry, University of Cambridge Clinical School, Hills Road, Cambridge, CB2 2QQ, England.

ABSTRACT The neurofibrillary tangles that occur in the brain in cases of senile dementia of the Alzheimer type contain a distinctive type of filament, the paired helical filament (PHF). We have developed a method for isolating the tangles postmortem in sufficient yield for structural study of PHFs by electron microscopy of negatively stained and shadowed preparations. This material shows the characteristic helical structure seen in sectioned embedded material. In addition, two striking fragmentation patterns are observed. (*a*) Some filaments show sharp transverse breaks at apparently random positions along the filament. (*b*) In a few PHFs one strand is missing for a variable length, whereas the other appears to maintain its structural integrity. The shadowed specimens show the PHF to be wound in a left-handed manner. These observations indicate that the PHF consists of subunits of very limited axial extent arranged along two left-handed helical strands. The visualization of the substructure within the PHFs is rather variable and a model building approach has therefore been adopted, which has allowed the main features seen in the images to be interpreted. The subunit appears to have at least two domains in a radial direction and an axial extent of <5 nm. The whole structure can best be described as a twisted ribbon and indeed alkali treatment does untwist PHFs to give flat ribbons. The nature of the proposed model makes it most unlikely that the PHF is formed by a simple collapse of normal cytoskeletal elements, such as neurofilaments.

In dementias of the Alzheimer type, the main kinds of morphological lesion which occur in the brain are the neurofibrillary tangle, the neuritic plaque, and granulovacuolar degeneration (18). Of these, the presence of abundant tangles in the cerebral cortex has an almost unequivocal diagnostic significance, being found only in cases with dementia (17). Lesions superficially similar to the tangle occur in other settings, such as aluminium intoxication (14), viral infections of the brain (24), and in cultured neurons treated with microtubule-depolymerizing agents (13). However, in Alzheimer's disease (6) and in some rarer neurological disorders (24), the tangles are distinctive in that the filaments which accumulate in the perikaryon of affected cells exhibit a characteristic paired helical structure. This appearance is different from any of the filamentous components of the normal neuronal cytoskeleton and from the filaments in other types of tangle (26). These paired helical filaments (PHFs)[1] are also found in the abnormal dendritic neurites of the neuritic plaque (7, 22). Thus, a morphologically distinctive class of filament, the PHF, occurs in the two main structural lesions of Alzheimer's disease. Strong statistical correlations have been established between the degree of dementia observed in life and the extent of plaque and tangle formation observed postmortem (3, 11, 12, 21). While such correlations do not establish causation, they do suggest that a better understanding of the nature and formation of plaques and tangles might provide insights into the pathogenesis of the disease. To this end we have been studying the structure of the PHF.

Previous electron microscopic studies of the structure of PHFs have been based mainly on sectioned material (7, 23). These showed that the PHF appeared to consist of two filaments wound helically around one another, with a longitudinal spacing between crossovers of ~65–80 nm and a width modulated between ~27–34 nm at the widest part and 10–15 nm at the narrowest. The dimensions reported for negatively stained PHFs are much smaller than those in sections, ranging from 15–22 nm at the widest to 6–8 nm at the narrowest (9,

[1] *Abbreviations used in this paper.* PHF, paired helical filament; PMSF, phenylmethylsulfonyl fluoride.

25). However, large numbers of free PHFs appear not to have been available for detailed structural analysis.

We have developed a preparative procedure that enables us to visualise large numbers of isolated PHFs by electron microscopy of shadowed or negatively stained specimens. The details of well-preserved filaments seen in these preparations and the nature of the fragmentation patterns observed suggested to us a preliminary model for the subunit organization in the PHF. We propose that the PHF consists of two strands of subunits interwound in a left-handed double helix; each subunit has a small (<5 nm) axial extent but has at least two domains in a radial direction. The nature of the subunit in the proposed model makes it unlikely that the PHF arises from a simple collapse of normal cytoskeletal elements.

MATERIALS AND METHODS

Source of Pathological Tissues: Brains were obtained postmortem from well-documented cases with a clinical diagnosis of senile dementia of the Alzheimer type. In each case, the clinical diagnosis was confirmed histologically by the presence of large numbers of plaques and tangles in frontal and temporal cortex. Tissues obtained from four human brains were used in the present study; these people had died at 65, 67, 71, and 84 years old. The material used in preparations was taken from frontal cortex, temporal cortex, and hippocampus. Transverse sections were cut after removal of pial and meningeal membranes. White matter was then dissected away and discarded, leaving 20–40 gm of tissue for use in an individual preparation. Tissues were stored at −70°C.

Preparation of PHF-enriched Fractions: Tissues were mixed with an approximately equal volume of 0.32 M sucrose, 1 mM magnesium chloride, 0.25 mM phenylmethyl sulfonyl fluoride (PMSF), 1 mM EGTA, 5 mM potassium phosphate (pH 6.5). The resulting mixture was homogenized in a teflon-glass manual homogenizer and filtered through a fourfold muslin screen mounted on a syringe, to give a final volume of 70–100 ml. The filtered homogenate was layered over an equal volume of 1.5 M sucrose, 1 mM magnesium chloride, 0.25 mM PMSF, 1 mM EGTA, 5 mM potassium phosphate (pH 6.5), and centrifuged at 27,000 *g* for 60 min in a Beckman SW 27 rotor (Beckman Instruments, Inc., Palo Alto, CA) at 15°C. The supernatant and pellet were discarded. The material at the interface was harvested, together with the underlying 1.5 M sucrose layer. This mixture was rehomogenized in a teflon-glass homogenizer, layered over 2.0 M sucrose, 1 mM magnesium chloride, 0.25 mM PMSF, 1 mM EGTA, 5 mM potassium phosphate (pH 6.5), and centrifuged at 40,000 *g* for 60 min in a Beckman SW 40 rotor at 15°C. The fraction that floated to the top and the upper supernatant were discarded, as was the bottom pellet. The material at the interface was harvested, resuspended in the initial 0.32 M sucrose and buffer solution, and centrifuged at 40,000 *g* for 60 min in a Beckman SW 40 rotor at 15°C. This final pellet was stored at −70°C, using the cut polyallomer centrifuge tube sealed with plastic film as a storage well.

Electron Microscopy: For electron microscopy, fragments of the final pellet were cut off and resuspended in 100 mM sodium chloride, 12.5 mM sodium phosphate (pH 6.5) using a 100-μl glass homogenizer. Typically, a 4-μl aliquot of this suspension was placed on a 400-mesh carbon-coated copper grid, generally washed with 2% lithium dodecyl sulphate, before negatively staining with 1% aqueous sodium phosphotungstate (pH 6) or with unbuffered 1% uranyl acetate. Micrographs were recorded at 80 kV at a nominal magnification of 45,000 using a Philips EM 301 electron microscope. Shadowing was performed in an Edwards evaporator (Edwards High Vacuum, Model E306A, Manor Royal, Crawley, Sussex, U.K.) using platinum deposited at an angle of about 20° for unidirectional methods and 5° for rotary methods.

RESULTS

Negatively Stained Filaments

A series of discontinuous sucrose gradient centrifugation steps was used to produce a fraction enriched in tangles and tangle fragments. This enrichment resulted from the removal of a substantial quantity of myelin-associated material during the flotation step (second centrifugation) and the pelleting of nuclei in both first and second centrifugations. Stages in the preparation of PHFs were monitored by counts of whole tangles and tangle fragments, using the distinctive gross morphology of tangles observed by fluorescence microscopy (27). Typical yields of tangle-like aggregates of PHFs seen in the electron microscope do not provide an index of purity, but in practice free PHFs could be found on almost all grid squares and PHF aggregates could be found in approximately one quarter of grid squares. The various cases and brain regions used in preparations showed no differences, either in terms of tangle morphology or PHF ultrastructure as seen by electron microscopy. No distinction between cases or source of tissue will therefore be made in the results reported here, although there was no pooling of material.

PHFs could be visualized with a number of negative stains, of which uranyl acetate and sodium phosphotungstate proved most useful. Uranyl acetate gave images with high contrast and clearly defined boundaries, whereas phosphotungstate gave superior delineation of the substructure. A typical fragment of tangle is shown in Fig. 1 *b*. Enlarged views (Fig. 1, *a* and *c*) of the PHFs projecting around the periphery show their appearance in sodium phosphotungstate stain. Fig. 2 *a* shows PHFs negatively stained with uranyl acetate.

In both stains the helical morphology was clear and showed the characteristic modulation in transverse diameter with a period of ~70 nm. However, the longitudinal periodicity was variable, ranging from 60 nm at one extreme to almost complete flattening and loss of modulation at the other. This will be discussed further below. The maximum diameter was also variable, ranging from 15 to 22 nm. The higher figure was less than that reported from sectioned embedded tissues (23) but comparable with previous negative staining (9, 25).

Fragmented Filaments

An important insight into the molecular architecture of the PHF is provided by two kinds of fragmentation pattern observed in negatively stained preparations.

A fairly common form of fragmentation arises from sharp transverse breaks across the filament. Infrequently, it is possible to find small areas of the grid in which extensive breakage of filaments has occurred to give an assortment of fragments (Figs. 2 *b* and 3 *a*). Additionally, there are instances of filaments fragmenting in situ, so that the relative disposition of the fragments is preserved (Figure 3 *b*). In both cases the fragments vary in length and there does not appear to be a favored longitudinal unit. Rather, PHFs appear to be able to break randomly at any point along their length. Importantly, a clean transverse break is almost invariably observed. Furthermore, in the shortest fragments which are still recognizable as originating from PHF (~30 nm in length), the basic helical twist characteristic of PHFs is well preserved.

Another kind of fragmentation which is much more rarely observed (Fig. 4, *a–c*) is a longitudinal break along the axis of the filament, with the splitting off and loss of half a PHF. It is particularly interesting that the single strand left after such a break continues to have an observable twist, retaining the same periodicity and substructure as the complete PHF. The example shown in Fig. 4 *b* is particularly striking, as the region of single strand is flanked by regions of apparently normal PHF. Although the straight transverse break is by far the most common ending for a PHF, occasionally a single strand can be seen extending for a short distance beyond a half break (Fig. 4, *d–f*) as previously noted (23). The single strand continues to show the same characteristic twist and periodicity as observed in the parent filament. The loss of one strand and

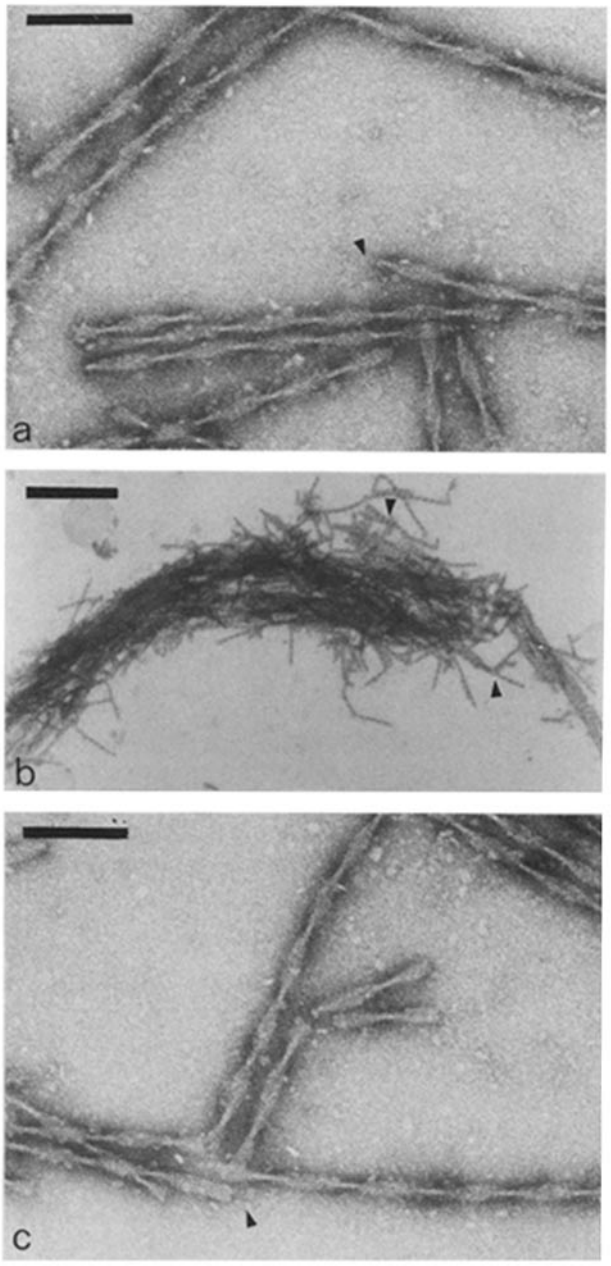

FIGURE 1 Fragment of a tangle, negatively stained with sodium phosphotungstate. A low magnification view is shown in *b*, whereas *a* and *c* show selected areas at higher magnification. Arrowheads identify corresponding points in the field. The characteristic morphology of the PHFs emerging from the tangle is clear. Bars, (*a* and *c*) 100 nm; (*b*) 1,000 nm. (*a* and *c*) × 135,000; (*b*) × 12,000.

the continuation of the other gives the end of the PHF a notched appearance. We have seen just one example (Fig. 4*g*) of an apparent internal transverse break in one of the strands of a PHF, associated with separation of the strands.

The conclusion that we draw from these fragmentation patterns is that each strand of a PHF can maintain its structural integrity. However, a half filament is probably much more prone to breakage than a complete PHF and therefore these structures are rarely observed. The sharp transverse fragmentation at apparently random positions with no sign of fraying (apart from the splitting just described) indicates that the constituent subunit is likely to be of limited axial extent and not an extended fibrous molecule.

Metal Shadowing

Metal shadowing gives a complementary view of the structure of the PHF. The unidirectionally shadowed material (Fig. 5*a*) shows that PHFs are left-handed. The clear sinusoidal modulation observed along the edge of the shadow implies that the cross section cannot be circular, but is instead typical of the varying aspect presented by a twisted ribbon-like structure. This interpretation is reinforced by the rotary-shadowed specimens (Fig. 5*b*).

Detailed Substructure

To aid description, the widest portion in the image of a PHF will be termed the "loop" and the narrowest portion the "crossover." A common feature of loops is the appearance of two pairs of longitudinal striations, one on either side of the axis (Fig. 6), as has been noted in another study (25). These striations consist of a pair of lighter lines, due to exclusion of stain, separated by a darker line of stain to give a "tramline" appearance. The pairs, or tramlines, on either side of the axis are further separated by a darker line along the axis, thus making two pairs of tramlines. The dark line along the axis is often darker than that within a tramline. The transverse separation of these four major longitudinal striations is ~4 nm. These striations do not generally extend the full length of a single loop. Rather, the loop has a polar appearance, with four light strands and a dark central line at one end, and three light strands, one of which is central, at the other.

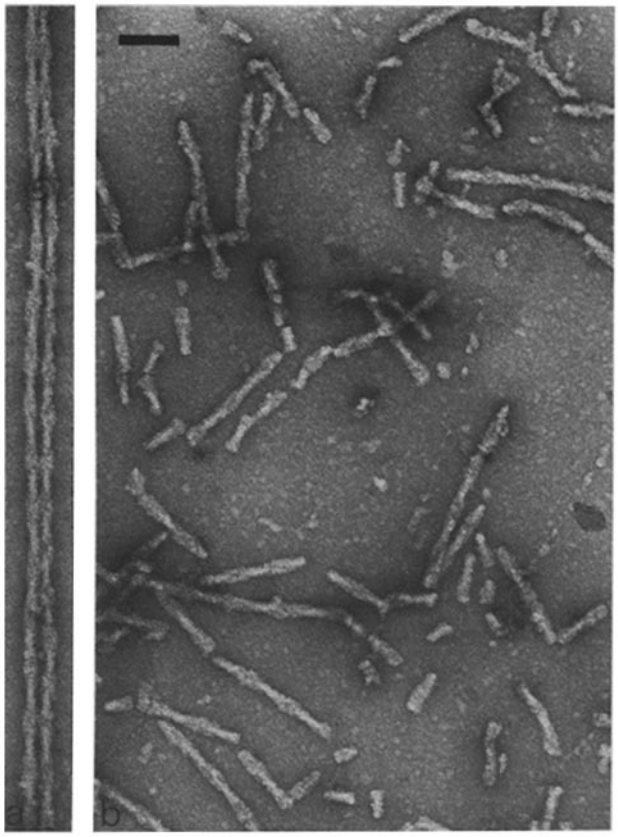

FIGURE 2 Intact and transversely fragmented PHFs, negatively stained with uranyl acetate. The filaments show higher contrast and sharper boundaries but less detailed substructure than the phosphotungstate-stained ones (Figs. 1 and 3). The sharp transverse breaks giving small fragments of apparently random lengths are clear. Bar, 100 nm. × 75,000.

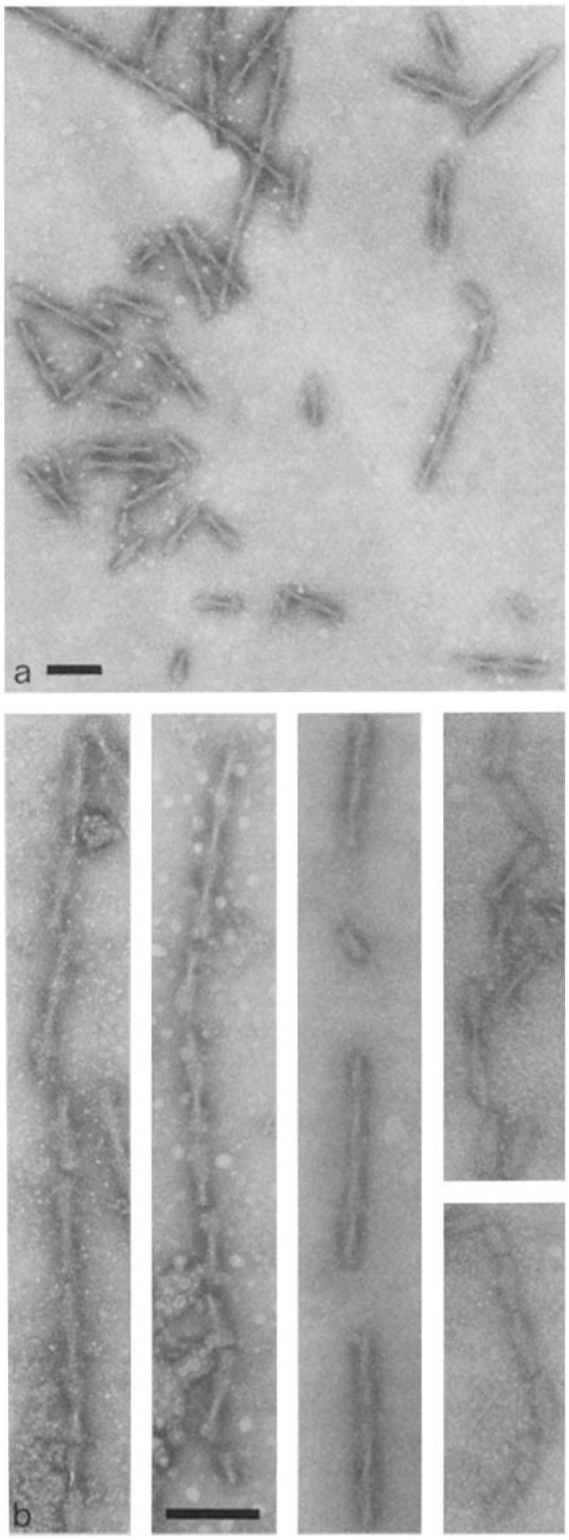

FIGURE 3 Transversely fragmented PHFs, stained with sodium phosphotungstate. *a* shows a field of fragments, whereas *b* shows individual PHFs which have broken with clear transverse breaks at apparently random positions along each filament. Bars, 100 nm. (a) × 75,000; (*b*) × 135,000.

Another common appearance of loops is shown in Fig. 7. The tramlines on either side of the axis appear to twist and fold under the other half filament, at either end of the loop. We call this a "strapwork" appearance. When the strapwork appearance is particularly pronounced, a thin sloping black line of stain can often be seen running from bottom left to top right across the loop. The strapwork and sloping line can both be produced in the model image (see *Model Building*) by reducing the weight of the front relative to the back of the helix, thus simulating partial stain-embedding. For a partially stain-embedded specimen it is usually the side nearest the carbon film which is contrasted, whereas in a shadowed specimen the side away from the carbon film is visualized. The shadowed and the partially stained (strapwork) images should therefore appear to be of opposite hand and this is what we observe.

A further feature of loops is the appearance of transverse

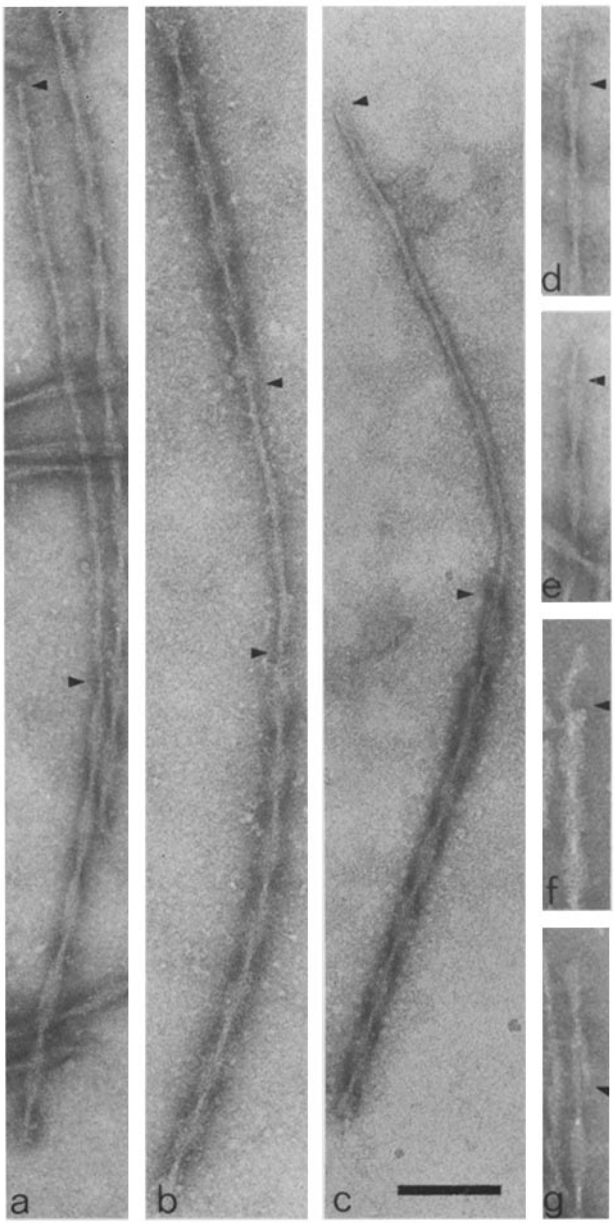

FIGURE 4 Longitudinal splitting of PHFs. a–c show PHFs that contain long regions of single rather than paired filament. The arrow heads indicate the ends of each single filament region, which in the case of *b* is in the middle of a PHF. *d–f* show short regions of single filaments at the ends of PHFs, giving these ends a notched appearance indicated by the arrowhead. *g* shows an example of an apparent internal break in one of the filaments constituting a PHF. All filaments were stained with sodium phosphotungstate. Bar, 100 nm. × 135,000.

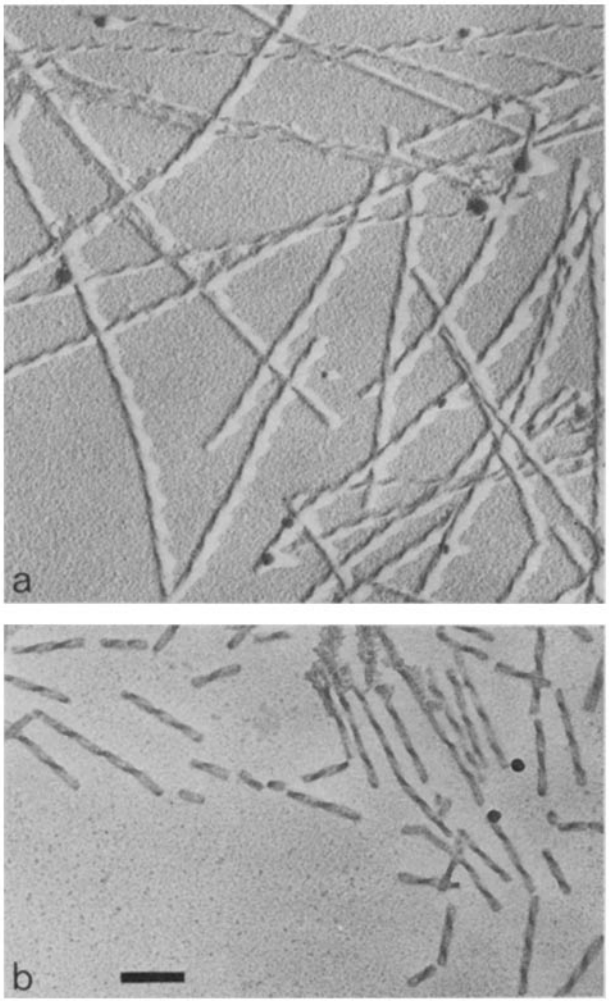

FIGURE 5 Shadowed PHFs. (*a*) Unidirectionally shadowed, showing clearly that the major helix is left handed. The strongly scalloped edges of the shadows indicate the changing aspect of the profile of the filament. (*b*) Rotary-shadowed, giving an impression of a twisted ribbon. Bar, 100 nm. × 75,000.

striations at an axial spacing of 3–4 nm (Fig. 8). Although individual loops showing this appearance are not uncommon, it is infrequent for adjacent loops to show it, even where the loop length remains constant. Also, transverse striations can sometimes be observed on one side of the axis, but not on the other, and occasionally these transverse striations can be seen to alternate on either side of the axis.

These diverse appearances are unlikely to be due to filament heterogeneity, since the various loop features described can often be discerned along the same stretch of filament. Rather, differences in stain penetration, filament preservation, and aspect presentation probably accentuate particular facets of a common underlying structural unit.

The appearances of crossovers are less diverse than loops. Generally, two principal strands can be discerned at crossovers, with a degree of stain accumulation on either side which is greater than that around loops. Frequently, an additional fainter strand can be detected within this region of stain build-up, on either side of the crossover.

Ribbon-like Structures

After an alkaline wash (1 M NaOH), untwisting of PHFs was observed, so that some filaments of very much longer

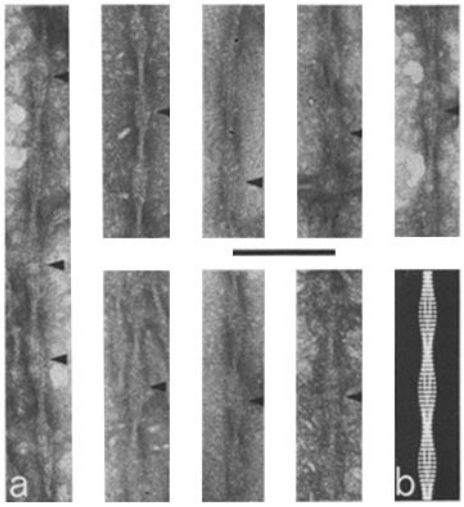

FIGURE 6 Substructure within loops. The arrowheads indicate loops in which the transition from three to four longitudinal white striations is visible (see text). This is most clearly seen by tilting the diagram so as to view each filament at a glancing angle along the direction of the axis. *b* shows a view of the model which displays similar features. In this and all subsequent figures the PHFs are negatively stained with sodium phosphotungstate. Bar, 100 nm. × 135,000.

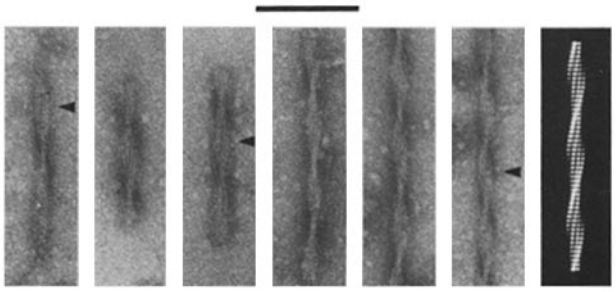

FIGURE 7 The strapwork appearance (see text). Loops in which the sloping black line is clearly visible are indicated by arrowheads. The far right panel shows the appearance of the model, when simulating partial stain embedding. Bar, 100 nm. × 135,000.

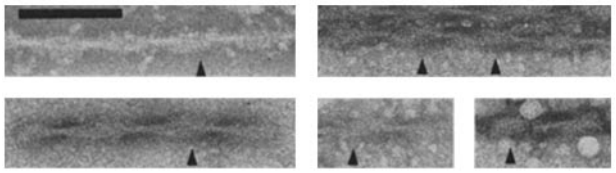

FIGURE 8 Transverse striping within loops. The arrowheads indicate loops which show particularly clear transverse striping of ~4 nm spacing. Bar, 100 nm. × 135,000.

periodicity and even entirely flattened ribbons were produced (Fig. 9). Ultrastructurally, the ribbons have a similar appearance to the loops in helical filaments described above. Some ribbons show transverse striations for variable distances. The most prominent pattern however is that of two pairs of longitudinal stripes, separated by a darker central cleft—the two sets of tramlines referred to earlier (see *Detailed Substructure*). Occasionally cleavage is observed along this central cleft to produce two half-ribbons. The example shown in Fig. 9*c* has one set of tramlines projecting a short distance beyond the other set and is analogous to the notched ends shown in Fig. 4, *d–f*. Furthermore, it contains a region of single strand joining the ribbon to the more normal part of the PHF. It is

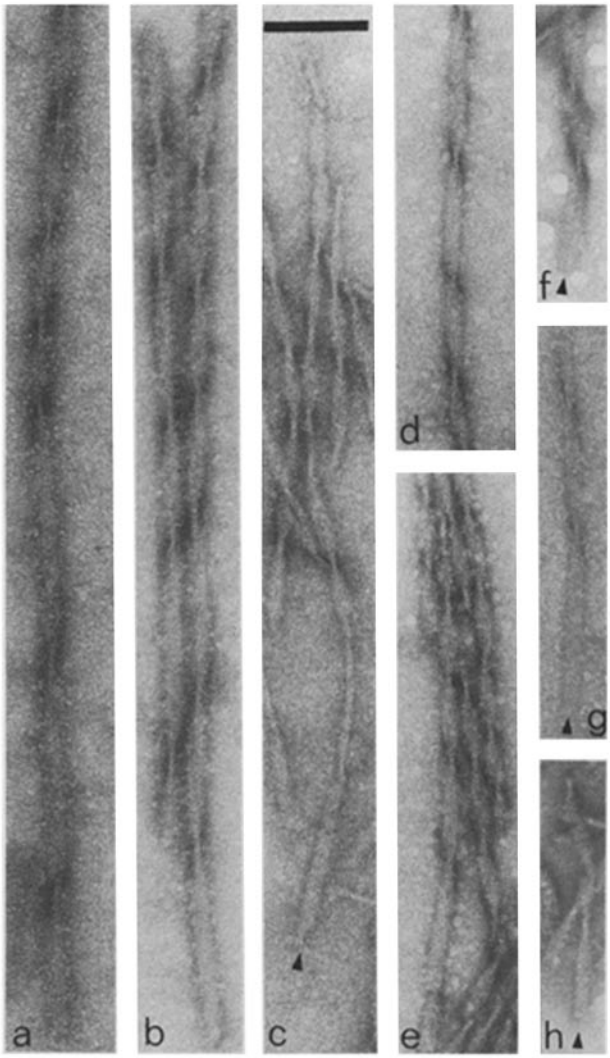

FIGURE 9 Flattened ribbons. PHFs washed with 1 M NaOH on the grid appear to untwist, to give a much greater distance between crossovers than in normal PHFs and hence extensive stretches in which the structure is displayed as a flattened ribbon. *a*, *b*, *d*, and *e* show general views of partially untwisted PHFs. The arrowheads in *c*, *f*, *g*, and *h* indicate stretches of ribbon where the two sets of tramlines separated by a strong central black line can be clearly seen (see text). Bar, 100 nm. × 135,000.

important to note that we do not see any splitting of the tramlines themselves into individual 4-nm substrands or protofilaments, either in the flattened ribbons or in the single-stranded notched ends of PHFs.

Model Building

In view of the variable appearance of the images of PHFs and the difficulty in obtaining sufficiently regular specimens to enable the production of good diffraction patterns, we have used model building in the first instance to interpret the micrographs. This was done by a computer program which generated structures with a specified helical symmetry, forming the subunits in the simplest way out of a set of spheres of variable size, density, and relative position. The results were viewed as projections on a raster-graphics terminal (AED 767), which could also be photographed.

It was possible to produce by trial and error a model (Fig. 10) which displays the major features described above in images of PHFs. The simplest obvious symmetry was assumed, namely that the two strands of the PHF were parallel and related by a twofold rotation parallel to the axis of the helix. The structure thus generated is polar, in agreement with the images (Fig. 6). The helical symmetry was chosen to make each strand repeat after 34 subunits per turn, though the whole model repeats in half this distance, corresponding to one loop. For a crossover spacing of 70 nm, this gives the subunit an axial dimension of ~4 nm, in agreement with the transversely striped images (Fig. 8). Changes in the assumed helical twist alter the length of the loop but do not significantly affect the internal details.

At each level, the pair of twofold related subunits were represented by a set of six spheres (Fig. 10*e*). The sizes and relative positions of the spheres were selected to give a model of the PHF with approximately the dimensions observed in the electron micrographs of negatively stained material. A minimum of two spheres in each subunit is needed to produce

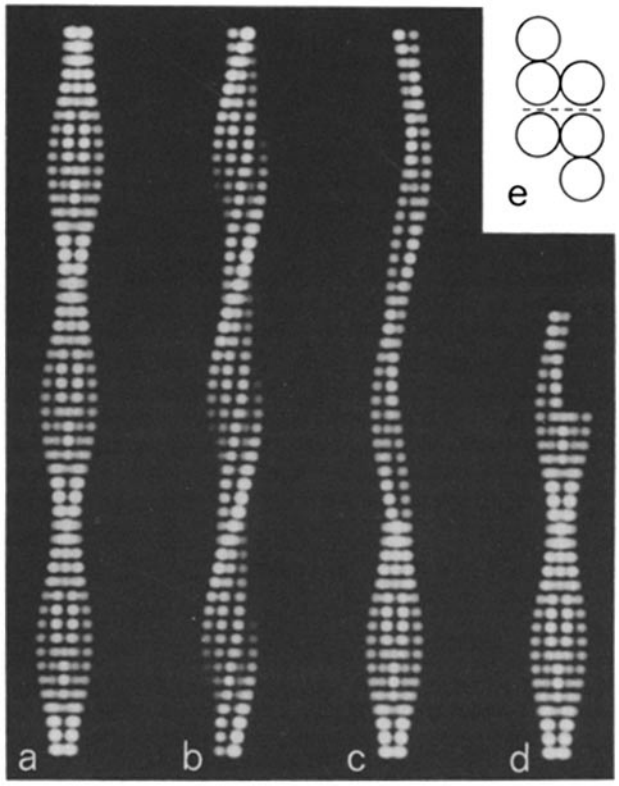

FIGURE 10 Simulated images of PHFs generated by computer modeling. (*a*) Complete PHF generated from the subunits shown in *e*. The polar character of each loop going from central white stripe to central dark stripe is clear. (*b*) Image arising from the same structure as *a* but with the weight of the near side of the helix reduced relative to that of the far side, thus simulating a one-sided appearance like the partially stain-embedded strapwork images (Fig. 7). In the convention adopted, this is equivalent to viewing the structure from the inside; a view from outside, such as is provided by shadowing, would give a mirror image to the one shown. (*c*) Transition from double strand (*bottom loop*) to single strand (*top two loops*) produces an image like those shown on Fig. 4, *a–c*, in which one strand of the PHF is missing. (*d*) By breaking one strand in the middle of a loop and allowing the other strand a short extension, a notched appearance is generated (cf. Fig. 4, *d–f*). (*e*) Cross section of the model showing the disposition of the spheres used to build the two subunits at a given level. The dotted line indicates the most likely boundary between physical subunits, based on the appearance of single strand regions.

the double tramline appearance in loops. However, models based on subunits with only two spheres gave images which looked far too empty compared with the micrographs. Addition of a third sphere to each subunit produced images much more like the micrographs. The likely boundary between physical subunits, based on the appearance of single-stranded regions, is indicated by the dotted line in Fig. 10*e*. Each physical subunit therefore has a stain-penetrated cleft, which gives rise to the tramline appearances. Though it would be possible to further refine the model, the basic form of which appears correct, a more productive approach is to use image reconstruction techniques; this is what we are attempting to do.

The best current model (Fig. 10*a*), besides displaying the overall wide-to-narrow modulation in diameter, shows internal details similar to those seen in images of PHFs. In particular, the change within a loop from a central white stripe (the 3-strand appearance) to a central dark stripe (the 4-strand appearance arising from two pairs of tramlines (cf. Fig. 6) is clear. By varying the densities of the elementary spheres as a function of depth in the direction of view, a partially one-sided appearance can be produced (Fig. 10*b*). This is very like the strapwork appearance (Fig. 7), and suggests that the latter arises from the PHF being only partially embedded in stain. The one-sided view also allows comparison with the shadowed images, which show similar features although of opposite hand, as discussed above. Finally, by suppressing a length of one of the helical strands, the transition from double to single strand can be mimicked (Fig. 10*c*), as can the nicked end of a loop with one strand projecting (Fig. 10*d*).

DISCUSSION

We have developed a protocol for preparing tangle-enriched fractions from cortical tissues obtained postmortem from Alzheimer cases. Filaments having the typical morphological characteristics of PHFs were visualized by electron microscopy using negative staining and metal shadowing. They were observed both as individual filaments and within larger aggregates having the appearance of intact or fragmented tangles. It is not clear at this stage to what extent the individual PHFs may have been degraded in the course of the procedures required for clear visualization, but the images produced do not look markedly different from the individual PHFs seen in embedded and sectioned material (10, 23).

Images of negatively stained and shadowed PHFs prepared in the manner described above seem to show more detail than can be seen in micrographs of sectioned embedded specimens. However, the details seen do not usually extend over adjacent lengths of the same filament. Rather, a pattern seen in one loop of a given filament, while not being seen in neighboring loops on that filament, can readily be found in individual loops of other filaments. In view of this diversity of appearance, probably arising from the preparative treatment and variation in helical twist rather than reflecting an intrinsic heterogeneity of the subunit packing, we have attempted initially to interpret the images by model building.

The structure that we propose is based on a left-handed double helix of subunits. The inherent double-helical nature of the packing is supported not merely by the overall "paired helical filament" appearance, but more importantly by the observation of single helical regions, both at broken ends and internally, in otherwise normal PHFs. It follows that the longitudinal contacts along a single helix are sufficient to maintain structural integrity. The further observation of sharp transverse breaks at apparently random positions along PHFs shows that the subunit is of fairly limited axial extent. Although we see a splitting of the PHF into individual strands of subunits, as described above, we do not see further fraying of these half PHFs into finer protofilaments. Thus it appears that in the axial direction the subunit is compact rather than extended or fibrous. We tentatively ascribe the 3–4-nm transverse banding seen in many images to the axial dimension of the subunit.

The longitudinal striping seen in loops, described above as two pairs of tramlines, is a consequence of the lining up of a domain-like substructure within the subunit and probably does not reflect the presence of structural protofilaments. The relative crudeness of the model does not allow firm identification, but it does appear that there must be at least two significant domains within the subunit to account for the staining patterns seen. We are presently attempting to produce an improved model of the structure by image reconstruction from the micrographs, and preliminary results confirm the basic correctness of the proposed model. From the overall size of the PHF we estimate that the structural subunit has dimensions of ~8 × 4 nm normal to the axis and 3–4 nm axially. This means that if it is a single chemical subunit it is likely to be of relatively high molecular weight. The structure can most easily be described geometrically as a twisted ribbon and models involving flattened or twisted tubules can be eliminated. The images of flattened ribbons produced by alkali treatment of PHFs confirm this interpretation.

Several studies have reported that antigens which cross-react with neurofilaments (4), and with the 210-kD neurofilament protein in particular (2, 5) are present in tangles. However the 210-kD component is not normally expressed in the cell body or apical dendrite of cortical or hippocampal pyramidal cells (16), where tangles typically appear. Furthermore, antibodies have been raised which label isolated tangles but which do not cross-react with neurofilaments (8, 20). It is clear from the pictures presented here that the individual strands of PHFs do not look like the published images of negatively stained neurofilaments (19) or intermediate filaments (1). Moreover, the shape and packing of the subunit proposed here makes it unlikely that the PHF derives either from a simple collapse or helical aggregation (10) or cross-linking (15) of complete neurofilaments. This does not exclude the possibility that PHFs derive from some component of neurofilaments, and it is clearly important to establish the biochemical nature of the subunit. If the subunit is related to a protein (e.g., the 210-kD protein) normally present in the cytoplasm of cortical pyramidal cells, it is likely that a specific change is required for its aberrant assembly into PHFs. Furthermore, this change would be the same in PHFs in the neurites of the plaque and in the tangle, in different regions of an affected cortex, and in different cases diagnosed histologically as having Alzheimer's disease.

We thank Pat Edwards for assistance with electron microscopy and shadowing, Claudio Villa for photographic printing, and Drs. Bennett, Butler, Finch, Klug, Kendrick-Jones, and Thøgersen for helpful suggestions and discussions.

C. M. Wischik was holder of a Commonwealth Medical Scholarship and is currently a Meres Senior Student at St. John's College, Cambridge, and a Lister Institute Research Fellow.

Received for publication 17 December 1984, and in revised form 25 February 1985.

REFERENCES

1. Aebi, U., W. E. Fowler, P. Rew, and T.-T. Sun. 1983. The fibrillar substructure of keratin filaments unraveled. *J. Cell Biol.* 97:1131–1143.
2. Anderton, B. H., D. Breiburg, M. J. Downes, P. J. Green, B. E. Tomlinson, J. Ulrich, J. N. Wood, and J. Kahn. 1982. Monoclonal antibodies show that neurofibrillary tangles and neurofilaments share antigenic determinants. *Nature (Lond.).* 298:84–86.
3. Blessed, G., B. E. Tomlinson, and M. Roth. 1968. The association between quantitative measures of dementia and of senile change in the cerebral grey matter of elderly subjects. *Br. J. Psychiat.* 114:797–811.
4. Gambetti, P., G. Shechet, B. Getti, A. Hirano, and D. Dahl. 1983. Neurofibrillary changes in human brain: an immunocytochemical study with a neurofilament antiserum. *J. Neuropathol. & Exp. Neurol.* 42:69–79.
5. Ihara, Y., N. Nukina, H. Sugita, and Y. Toyohura. 1981. Demonstration of 210 K neurofilament antigen in neurofibrillary tangles of Alzheimer's disease. *Proc. Jpn. Acad.* 57(B):152–156.
6. Kidd, M. 1963. Paired helical filaments in electron microscopy of Alzheimer's disease. *Nature (Lond.).* 197:192–193.
7. Kidd, M. 1964. Alzheimer's disease—an electron microscopical study. *Brain* 87:307–320.
8. Ihara, Y., C. Abraham, and D. J. Selhoe. 1983. Antibodies to paired helical filaments in Alzheimer's disease do not recognize normal brain proteins. *Nature (Lond.).* 304:727–730.
9. Merz, P. A., R. A. Somerville, and H. M. Wisniewski. 1983. Abnormal filaments in scrapie and senile dementia of Alzheimer type. *In* Virus Non-conventionnels et Affections du Systeme Nerveux Central. L. A. Court, editor. Masson, Paris. 259–281.
10. Metuzals, J., V. Montpetit, and D. F. Clapin. 1981. Organization of the neurofilamentous network. *Cell Tissue Res.* 214:455–482.
11. Roth, M., B. E. Tomlinson, and G. Blessed. 1967. The relationship between quantitative measures of dementia and of degenerative changes in the cerebral grey matter of elderly subjects. *Proc. R. Soc. Med.* 60:254–260.
12. Roth, M. 1971. Classification and etiology in neural disorders of old age: some recent developments. *In* Recent Developments in Psychogeriatrics. D. W. Kay and A. Walk, editors. Hadley Bros. Ltd., Kent. 1–18.
13. Sato, Y., S. U. Kim, and B. Ghetti. 1982. Neurofibrillary tangle formation in cultured neurons. *J. Neuropathol. & Exp. Neurol.* 41:341.
14. Selkoe, D. J., R. K. Liem, S. H. Yen, and M. L. Shelanski. 1979. Biochemical and immunological characterization of neurofilaments in experimental neurofibrillary degeneration induced by aluminium. *Brain Res.* 163:235–252.
15. Selkoe, D. J., C. Abraham, and Y. Ihara. 1982. Brain transglutaminase: in vitro cross-linking of human neurofilament proteins into insoluble polymers. *Proc. Natl. Acad. Sci. USA.* 79:6070–6074.
16. Shaw, G., M. Osborn, and K. Weber. 1981. An immunofluorescence microscopical study of the neurofilament triplet proteins, vimentin and glial fibrillary acidic protein within the adult rat brain. *Eur. J. Cell Biol.* 26:68–82.
17. Tomlinson, B. E. 1977. The Pathology of Dementia. In Dementia. C. G. Wells, editor. F. A. Davis Co., Philadelphia. 2nd edition. 113–153.
18. Tomlinson, B. E. 1979. The ageing brain. *In* Recent Advances in Neuropathology. No. 1. W. T. Smith and J. B. Cavanagh, editors. Churchill Livingstone, London. 129–159.
19. Wais-Steider, C., P. A. M. Eagles, D. S. Gilbert, and J. M. Hopkins. 1983. Structural similarities and differences amongst neurofilaments. *J. Mol. Biol.* 165:393–400.
20. Wang, G. P., I. Grundke-Iqbal, R. J. Kascsak, and H. M. Wisniewski. 1984. Alzheimer neurofibrillary tangles: monoclonals to inherent antigens. *Acta Neuropathol.* 62:268–275.
21. Wilcock, G. K., and M. M. Esiri. 1982. Plaques, tangles and dementia: a quantitative study. *J. Neurol. Sci.* 56:343–356.
22. Wisniewski, H., and R. Terry. 1970. An experimental approach to the morphogenesis of neurofibrillary degeneration and the argyrophilic plaque. *In* Alzheimer's Disease and Related Conditions. G. W. Walstenholme and M. O'Connor, editors. Churchill, London. 223–248.
23. Wisniewski, H. M., H. K. Narany, and R. D. Terry. 1976. Neurofibrillary tangles of paired helical filaments. *J. Neurol. Sci.* 27:173–181.
24. Wisniewski, K., G. A. Jervis, R. C. Moretz, and H. Wisniewski. 1979. Alzheimer neurofibrillary tangles in diseases other than senile and presenile dementia. *Ann. Neurol.* 5:288–294.
25. Wisniewski, H. M., P. A. Merz, and K. Iqbal. 1984. Ultrastructure of paired helical filaments of Alzheimer's neurofibrillary tangle. *J. Neuropathol. & Exp. Neurol.* 43:643–656.
26. Yagishita, S., Y. Itol, W. Nan, and N. Amano. 1981. Reappraisal of the fine structure of Alzheimer's neurofibrillary tangles. *Acta Neuropathol.* 54:239–246.
27. Yen, S.-H. C., F. Gaskin, and R. D. Terry. 1981. Immunocytochemical studies of neurofibrillary tangles. *Am. J. Pathol.* 104:77–89.